Journal of Alloys and Compounds 509 (2011) 8105–8110

Contents lists available at ScienceDirect

Journal of Alloys and Compounds

journal homepage: www.elsevier.com/locate/jallcom

Hydrothermal synthesis of hexagonal and orthorhombic MoO_3 nanoparticles

A. Chithambararaj, A. Chandra Bose*

Nanomaterials Laboratory, Department of Physics, National Institute of Technology, Tiruchirappalli 620 015, India

ARTICLE INFO

Article history:
Received 24 November 2010
Received in revised form 13 May 2011
Accepted 17 May 2011
Available online 26 May 2011

Keywords:
Hydrothermal method
Hexagonal phase
Orthorhombic structure
Phase transformation
K–M function

ABSTRACT

Molybdenum oxide (MoO_3) with two different crystal structures (hexagonal and orthorhombic) was successfully synthesized by an effective and environmental friendly hydrothermal method. The phase confirmation and structural properties of the sample was elucidated by X-ray diffraction (XRD) method. The reaction temperature has great impact on the crystal structure, size, shape and chemical composition of the samples. Vibration behavior of chemical bonds was characterized by Fourier transform infrared spectroscopy (FT-IR) and the observed peaks confirm the formation of MoO_3. Scanning electron microscopy (SEM) observation shows that an increase in reaction temperature, the shape was drastically changed from one dimensional (1D) to two dimensional (2D) layered structures. Energy dispersive X-ray analysis (EDX) reveals that the as-prepared samples are in non-stoichiometric composition and their composition varies with reaction temperature. The thermal study was acquired by thermo gravimetric analysis and it demonstrates the process of dehydration and deammonization, observed below 260 °C and phase transformation from hexagonal to highly stable orthorhombic phase at 400–450 °C. Additionally, the optical absorption properties were measured using diffuse reflectance spectroscopy (DRS) and the band gap energy, estimated from Kubelka–Munk function (K–M) was found to be in the range of 3.01–3.24 eV.

1. Introduction

Many physical properties of nanostructured materials depend strongly on their size, shape and crystal structure. Thus, the modern chemistry and material science have been highly focused on the development of precise architectural manipulation of nanocrystals with well defined crystal structure and tunable size [1]. The production of nanostructures with phase controlled procedure is still a challenge for material scientists and there is a great interest in developing new methods to adopt phase controlled synthesis. Recently, molybdenum oxide and its compounds have been focused due to their unusual physical and chemical properties in the nanoscale regime. Their unique structural and optical properties are being a promising material for various industrial applications such as catalysis, sensors, photo-chromic, electro-chromic devices, display materials and battery systems [2–6]. A variety of techniques have been developed to control the structure and morphology of MoO_3 material like sputtering, thermal evaporation, template synthesis, chemical synthesis and hydrothermal method [7–13]. Compared to the above mentioned methods, the hydrothermal method is the solution phase route, has been proven to be an effective and convenient process to fabricate new meta-stable structures with controlled size and dimension.

In this paper, we established a general strategy for the synthesis of MoO_3 with meta-stable (hexagonal) and stable (orthorhombic) crystal structures using hydrothermal method. The reaction temperature is varied and their effect on the crystal structure, shape and size are investigated. Synthesized samples are studied by XRD, TGA, FTIR and SEM to know the structural, functional and morphology of the resultant products. Further, Kubelka–Muck function is carried out to study the stoichiometric effects on the optical properties.

2. Experimental

2.1. Preparation

In a typical procedure for the preparation of MoO_3 nanoparticles, 0.2 M ammonium molybdate was added to 10 ml of distilled water. After vigorous stirring for 15 min, 5 ml of concentrate HNO_3 was introduced into the solution. The mixer solution was transferred into a teflon-lined stainless steel autoclave, sealed and maintained at different temperatures (T = 90, 150 and 210 °C) for 12 h. The obtained precipitates were separated by centrifugation, washed with ethanol and distilled water in sequence, and finally dried in vacuum at 70 °C for 12 h.

2.2. Characterization

XRD measurements were performed using Ultima III Rigaku X-ray diffractometer at a scanning rate of 0.2°/min in the range of 5–80° with Cu $K_{\alpha1}$ radiation (1.5406 Å). FT-IR measurements were carried out by Perkin Elmer, Spectrum RX1 spectrometer using KBr pellet technique. SEM micrographs and EDX analysis were obtained using SEM (S4800 Hitachi). The thermal behavior was analyzed using EXS-

* Corresponding author. Tel.: +91 431 2503605; fax: +91 431 2500133.
E-mail address: acbose@nitt.edu (A.C. Bose).

0925-8388/$ – see front matter © 2011 Elsevier B.V. All rights reserved.
doi:10.1016/j.jallcom.2011.05.067

TAR6200 thermal analyzer at a heating rate of 10 °C/min from room temperature to 550 °C. The weight loss, mass differential and thermal differential were observed from thermo gravimetric (TG), differential thermo gravimetric analysis (DTG) and differential thermal analysis (DTA). The optical properties were studied using DRS and were recorded using a computer controlled T90+ UV/Vis spectrophotometer. A $BaSO_4$ plate was used as a reference (100% reflectance), on which a fine ground powder of the sample were pressed. The spectra were recorded at room temperature in the wavelength range of 230–800 nm with the speed of 1 nm/s.

3. Results and discussion

3.1. Crystal structure analysis

The XRD pattern of the samples synthesized for different reaction temperatures (T = 90, 150 and 210 °C) are displayed in Fig. 1. It is clearly observed that the MoO_3 crystal has different phase as a function of hydrothermal reaction temperature. At 90 °C, it favors the formation of pure hexagonal MoO_3 (JCPDS – 21-0569) (Fig. 1a), whereas at 150 °C, the product comprises of hexagonal and orthorhombic phases (Fig. 1b). It is well noticed that there is a phase change transformation from hexagonal to more stable orthorhombic MoO_3 phase as the reaction temperature increases. Further increase in reaction temperature to 210 °C (Fig. 1c), a complete phase change from hexagonal to orthorhombic is observed. The obtained pattern is well matched with standard data file (JCPDS – 35-0569). It states that an increase in reaction temperature changes the pressure inside the reactor that provides sufficient surface free energy and internal energy to the growing nuclei. This energy difference prompt new crystal structures in the final product [14,15]. In Fig. 1c, the diffraction peaks along (0 b 0) has stronger intensity compared to the standard JCPDS data, indicating the orientation of particles along the b-axis and thus, resulting in anisotropic growth [16]. In addition, the increase in intensity indicates an improvement in the crystallinity of the product under hydrothermal condition. The crystallite size of the as-synthesized samples are calculated using the Debye–Scherrer equation [17]

$$D_{hkl} = \frac{K\lambda}{\beta_{hkl} \cos\ \theta_{hkl}} \quad (1)$$

where D_{hkl} is the crystallite size (nm), K is shape factor (0.9), λ is the wavelength of Cu $K_{\alpha 1}$ radiation (1.5406 Å), β_{hkl} is the full width at the half maximum (FWHM) intensity which is initially eliminated from the instrumental broadening using silicon as standard reference and θ_{hkl} is the Bragg's diffraction angle. The structural parameters including crystal phase, crystallite size and lattice parameters are tabulated in Table 1. From Table 1, one can observe that the growth of the MoO_3 particle is highly accelerated with the increase in reaction temperature and thus, enhances the crystallite size. The calculated lattice parameters values are comparatively lower than standard JCPDS data and can be attributed to the changes in size, shape, and non-stoichiometry [18] of the sample which is supported from following results. From Fig. 1d, a significant peak shift towards higher angle (2θ) value is observed at 25.7° implying a decreased lattice parameter. This deviation is a direct indication of compressive strain present in the MoO_3 material and thus the lattice parameter values are comparatively lower than the standard JCPDS value.

3.2. Functional group analysis

The functional groups present in the as-synthesized materials are identified by FT-IR analysis. Fig. 2 shows the vibrational spectra of MoO_3 in the spectral range of wavenumber 400–4000 cm^{-1}. Fig. 2a and b is the FT-IR spectra of MoO_3 samples prepared at T = 90 °C and 150 °C respectively. The peaks at 3550 cm^{-1} and 1618 cm^{-1} correspond to the stretching and bending vibration of hydrogen bonded –OH group water molecules, respectively.

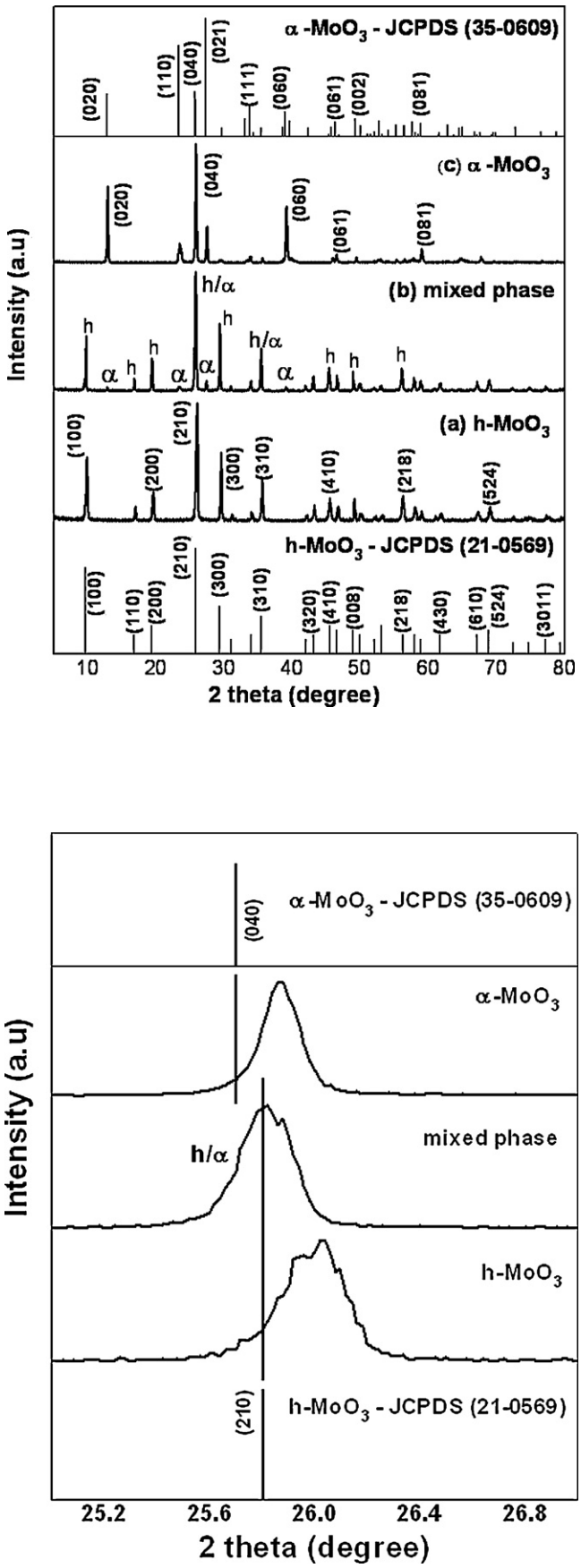

Fig. 1. (a–c) XRD pattern of MoO_3 synthesized at (a) 90 °C, (b) 120 °C and (c) 210 °C. (d) Peak shift variation in pure and mixed phase MoO_3 synthesized at different temperatures.

Table 1
Structural and optical properties of MoO_3 nanoparticles.

Reaction temperature	Crystalline phase	Crystallite size (nm)	Lattice parameters			O/Mo atomic ratio	band gap (E_g) (eV)
			a (Å)	b (Å)	c (Å)		
90 °C	Hexagonal (h)-MoO_3	49 nm	10.47 (10.53[a])	10.47 (10.53[a])	14.918 (14.876[a])	3.85	3.01
150 °C	Mixed phase (h/α)-MoO_3	60 nm	10.54/ 3.7874	10.54 /13.80	14.90/3.2521	3.10	3.24
210 °C	Orthorhombic (α)-MoO_3	82 nm	3.78 (3.962[a])	13.776 (13.85[a])	3.25 (3.697[a])	2.22	3.15

[a] Bulk value.

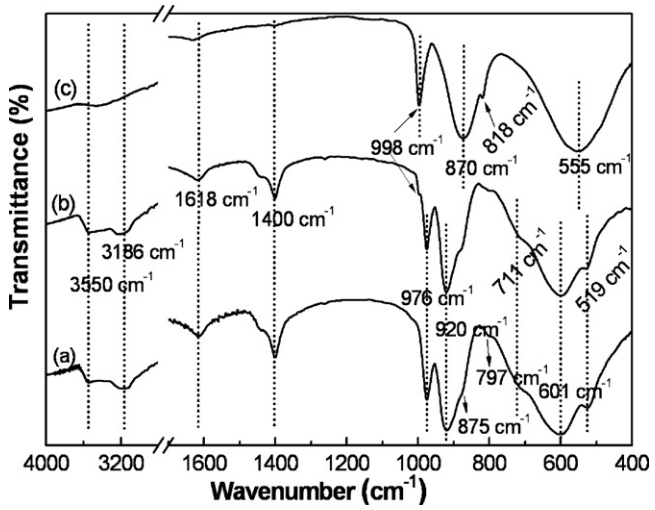

Fig. 2. (a–c) FT-IR vibrational spectra of MoO_3.

Similarly, the peaks at 3186 cm^{-1} and 1400 cm^{-1} are due to stretching and bending vibration of N–H of NH_4^+ groups. The observations are well consistent with the previous reported data [19,20]. It is well noticed in Fig. 2c (T = 210 °C) that there is no trace of –OH or N–H related absorption peaks. This is due to the absence of surface ligands in sample synthesized at higher reaction temperature [21]. The samples show absorption peaks in the region of 1000–400 cm^{-1} corresponding to stretching and bending vibrations of metal–oxygen characteristic bonds. In Fig. 2a, the vibrational peaks confirm the sample is single phase hexagonal (h)-MoO_3. The observed small intensity followed by high intensity peak at 978 cm^{-1} and 916 cm^{-1} are the characteristic of υ_s(Mo=O) stretching vibrations of hexagonal phase. The absorption peaks between 500 and 600 cm^{-1} correspond to the vibration of Mo–O bond [22]. Fig. 2b gives similar spectral band as h-MoO_3 and a small peak appears at 998 cm^{-1}, indicating the presence of secondary phase. Fig. 2c is FT-IR spectrum for orthorhombic (α)-MoO_3, shows sharp and broad peak in the region 1000–900 cm^{-1} attributed to stretching vibration of molybenyl bond υ_s(M=O). Another broad vibration band at 555 cm^{-1} is due to interaction of oxygen atom with three metal atoms υ(O–3Mo) [23]. From the above results, in Fig. 2b, the peak observed at 998 cm^{-1} is due to the existence of orthorhombic phase with hexagonal phase.

3.3. Micro-structure and elemental analysis

Fig. 3a–c is SEM micrographs, revealing the surface morphology and shape of the resultant products synthesized at various hydrothermal reaction temperatures. Sample synthesized at low

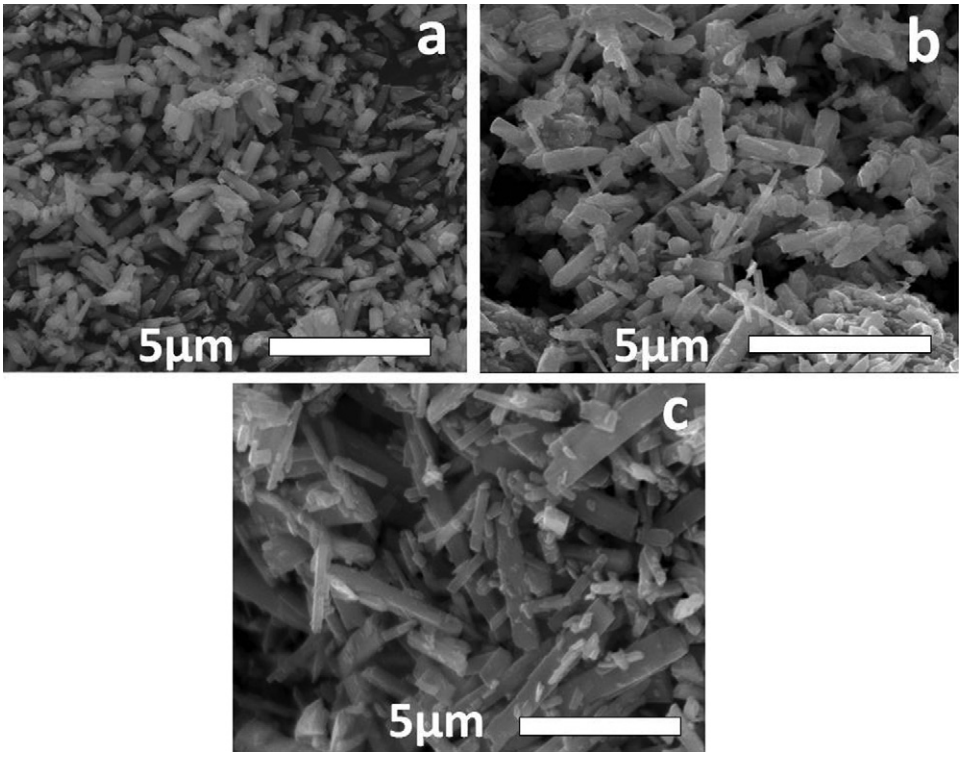

Fig. 3. (a–c) SEM images of MoO_3 synthesized at (a) 90 °C, (b) 120 °C and (c) 210 °C.

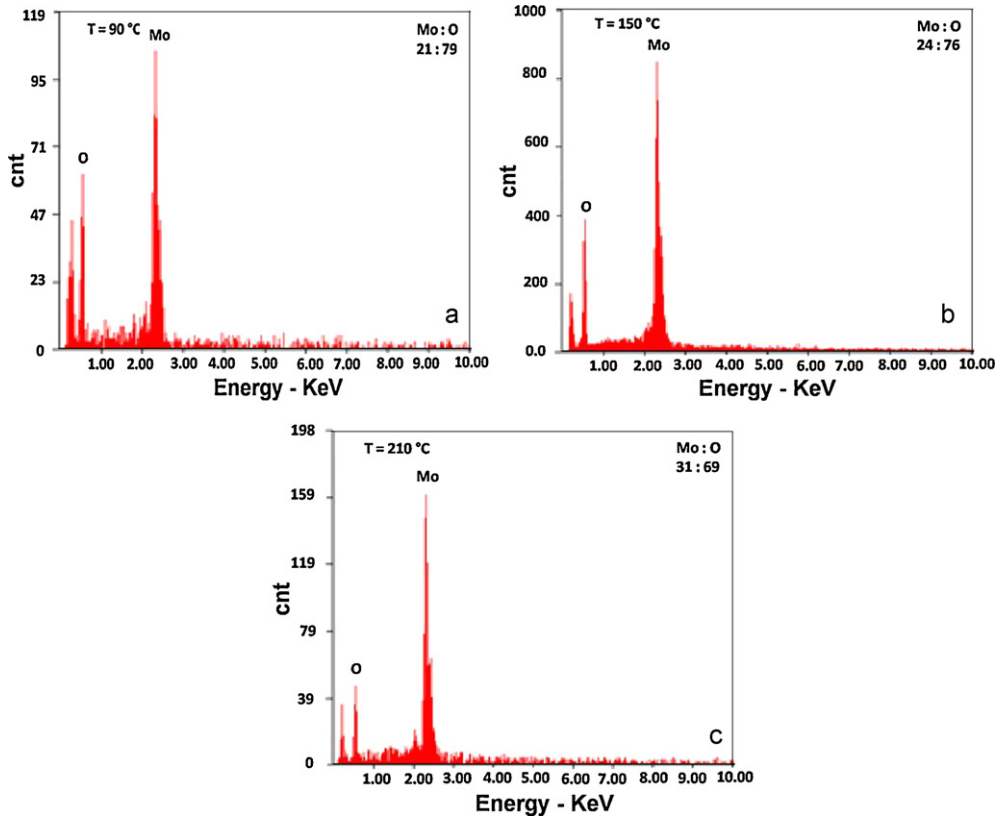

Fig. 4. (a–c) EDX analysis of MoO_3 synthesized by different reaction temperatures.

reaction temperature (Fig. 3a), exhibit hexagonal rods with diameter of 300 nm and length of several micrometers. When the reaction temperature increases to 150 °C (Fig. 3b) the particle growth is stimulated and thus particles are highly agglomerated. When $T = 210$ °C (Fig. 3c) there is a morphology change from hexagonal rods to layered structure. Thus, hexagonal rods formed at low temperature apparently grow in size and transformed to layered structure at higher hydrothermal reaction temperature. This anisotropic growth under hydrothermal reaction condition is due to several factors including the intrinsic structure features of specific faces, precursors, the foreign energy activation, and the autogenous pressure [14]. This favors preferable 1D rod and layered structure in the MoO_3 material. The elemental composition is analyzed using EDX results and the atomic ratio (O/Mo) is tabulated in Table 1. From Fig. 4a–c, it confirms that the samples are composed of only Mo and O, no trace of secondary impurities is observed. Interestingly, it is noted that the atomic percentage of oxygen decreases as increase in hydrothermal reaction temperature. Thus, it promotes MoO_3 with stoichiometric and non-stoichiometric compositions resulting in excess of oxygen and oxygen vacancies in the sample.

3.4. Thermal properties

The phase change in the as-synthesized pure and mixed phase MoO_3 material have been investigated using TG/DTG and DTA analysis by heating the samples up to 550 °C. Fig. 5a and b represents the TG/DTG curves for sample synthesized at $T = 90$ °C and $T = 150$ °C, respectively. The first weight loss up to 130 °C is due to the complete desorption of water molecules that are physically adsorbed on the surface. The second weight loss (at 230 °C) can be attributed to an elimination of ammonia (NH_3) from the MoO_3 sample [24]. Broad hump below 260 °C in DTA curve (Fig. 6a and b) representing the dehydration and deammonization process. After dehydration and deammonization process, sudden weight loss in TG and rise of sharp exothermic peak in DTA in the range of 400–420 °C is due to liberation of coordinated water and ammonia molecules from the internal structure of solid sample which promotes phase change of MoO_3 from hexagonal to orthorhombic structure [25,26]. Above 450 °C, no change in TG/DTA curve is observed revealing that the thermodynamically stable α-MoO_3 is attained. The powder subjected to TGA measurements are given for XRD and confirms the stable orthorhombic structure formed above 450 °C (figure not included). The sample synthesized at $T = 210$ °C (Figs. 5c and 6c), predicts no such decomposition process or phase transformation on heating. Thus, it confirms the absence of coordi-

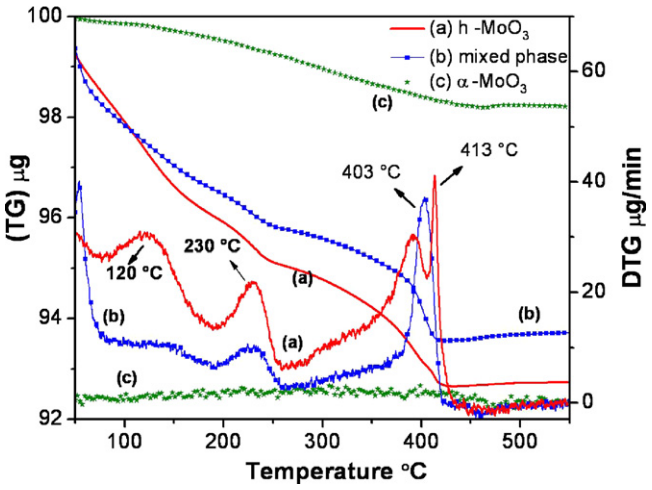

Fig. 5. (a–c) TG/DTG graph of MoO_3 prepared at (a) 90 °C, (b) 120 °C and (c) 210 °C.

Table 2
Weight loss and temperature range from TG and DTA measurements.

TG analysis	Hydrothermal reaction temperature					
	$T = 90\,^{\circ}C$		$T = 150\,^{\circ}C$		$T = 210\,^{\circ}C$	
	Temperature range (°C)	Weight loss (%)	Temperature range (°C)	Weight loss (%)	Temperature range (°C)	Weight loss (%)
Dehydration	75–190	2.52	75–190	1.71	–	
Deammonization	190–265	1.02	190–260	0.78	–	
Phase change	350–450	1.55	350–450	1.6	–	
Total weight loss (%)	7.3%		6.3%		1.8%	

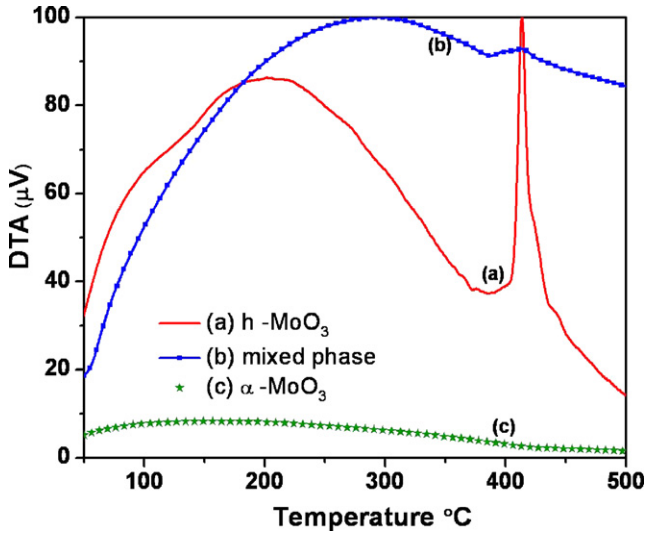

Fig. 6. (a–c) DTA curve of as-synthesized MoO_3.

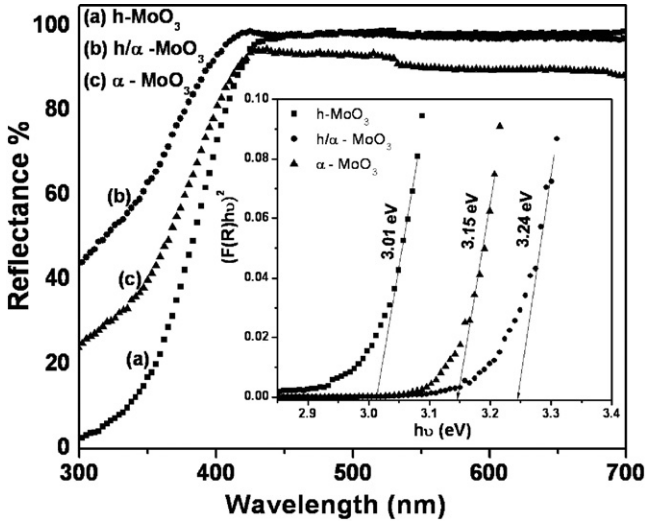

Fig. 7. (a–c) Diffuse reflectance spectra of as-synthesized MoO_3 and the inset is band gap energy of MoO_3.

nated water and ammonium ions and exhibits highly stable phase. The observed results well agreed with XRD results. The weight loss % and temperature range for dehydration, deammonization and phase transformation are summarized in Table 2.

3.5. Diffuse reflectance spectra

The optical absorption properties of the as-prepared MoO_3 materials are characterized by DRS measurement. Fig. 7a–c shows the reflectance spectra of sample synthesized at various reaction temperatures. The maximum reflectance of 95% is observed in the range of 800–450 nm due to weak absorption by the material. Below 450 nm, a fall in reflectance can be assigned to the fundamental absorption by the material which gives direct band to band (valance band to conduction band) transition [27]. The optical absorption co-efficient is evaluated using K–M function [28]

$$F(R_\infty) = \frac{(1-R_\infty)^2}{2R_\infty} = \frac{K(\lambda)}{s(\lambda)} \quad (2)$$

where $F(R_\infty)$ is the K–M function or re-emission function, R_∞ is the diffuse reflectance of an infinitely thick sample, $K(\lambda)$ is the absorption coefficient, $s(\lambda)$ is the scattering coefficient. For direct band gap transitions, the optical band gap value E_g is calculated using the relation [29] $(F(R_\infty)h\nu) = A(h\nu - E_g)^{1/2}$, where A is constant, $h\nu$ is the photon energy and E_g is the optical band gap. The E_g is determined by extrapolating the linear portion of the plot between $(F(R_\infty)h\nu)^2$ and $(h\nu)$ shown as an inset in Fig. 7. The band gap values are estimated and summarized in Table 1. From Table 1, the band gap value of MoO_3 synthesized at 150 °C shows higher band gap value (3.24 eV) and the samples synthesized at 90 °C and 210 °C gives low E_g values. Based on the XRD and EDX results, it is proposed that the pure hexagonal and orthorhombic phase contains grain boundary defects (interstitial oxygen or oxygen vacancy) which lead to non-stoichiometric behavior [19,30]. The MoO_3 synthesized at 150 °C is in mixed phase which consists of different crystallographic features. Further, the reflectance intensity decreased for sample synthesized at 210 °C is attributed to crystallite size effect on the scattering phenomenon. The increased crystallite size significantly decreases the scattering co-efficient and there by, reduce the reflectance intensity in the spectrum [28].

4. Conclusions

In conclusion, hydrothermal method is used to synthesize MoO_3 with two different phases (hexagonal and orthorhombic). The significant outcome of the study is the achievement of phase controlled MoO_3 through hydrothermal synthesis as a function of reaction temperature. The presence of metal–oxygen vibrational band is identified and located in the region of 1000–400 cm^{-1}. The morphology change from 1D hexagonal rod to layered structure is investigated and is found to be strongly dependent on reaction temperature. The phase transition from meta-stable hexagonal to stable orthorhombic α-MoO_3 phase is observed at 430 °C. The optical band gap is calculated based on K–M function and is in the range of 3.01–3.24 eV.

Acknowledgement

This research was financially supported by NRB-DRDO project (DNRD/05/4003/NRB/143), Government of India. We thank Dr. R. Justin Joseyphus for thermal studies.

References

[1] K.T. Yong, Y. Sahoo, M.T. Swihart, P.N. Prasad, J. Phys. Chem. C 111 (2007) 2447.
[2] A.M. Taurino, A. Forleo, L. Francioso, P. Siciliano, Appl. Phys. Lett. 88 (2006) 152111.
[3] B. Yen, Z. Zheng, J. Zhang, H. Gong, Z. Shan, W. Huang, T. Yu, J. Phys. Chem. C 113 (2009) 20259.
[4] W. Li, F. Cheng, Z. Tao, J. Chen, J. Phys. Chem. B 110 (2006) 119.
[5] S. Hamwi, J. Meyer, T. Winkler, T. Riedl, W. Kowalsky, Appl. Phys. Lett. 94 (2009) 253307.
[6] D. Mariotti, H. Lindstrom, A.C. Bose, K. Ostrikov, Nanotechnology 19 (2008) 495302.
[7] X. Chen, W. Lei, D. Liu, J. Hao, Q. Cui, G. Zou, J. Phys. Chem. C 113 (2009) 21582.
[8] Y. Zhao, J. Liu, Y. Zhou, Z. Zhang, Y. Xu, H. Naramoto, S. Yamamoto, J. Phys. Condens. Matter 15 (2003) L547.
[9] G. Li, L. Jiang, S. Pang, H. Peng, Z. Zhang, J. Phys. Chem. B 110 (2006) 24472.
[10] Q.P. Ding, H.B. Huang, J.H. Duan, J.F. Gong, S.G. Yang, X.N. Zhao, Y.W. Du, J. Cryst. Growth 294 (2006) 304.
[11] C.V. Subba Reddy, E.H. Walker, C. Wen, S. Mho, J. Power Sources 183 (2008) 330.
[12] L. Fang, Y. Shu, A. Wang, T. Zhang, J. Cryst. Growth 310 (2008) 4593.
[13] X.W. Lou, H.C. Zeng, Chem. Mater. 14 (2002) 4781.
[14] Y.P. Fang, A.W. Xu, A.M. Qin, R.J. Yu, Cryst. Growth Des. 5 (2005) 1221.
[15] W. Avansi, C. Ribeiro, E.R. Leite, V.R. Mastelaro, Cryst. Growth Des. 9 (2009) 3626.
[16] H.C. Zeng, J. Cryst. Growth 186 (1998) 393.
[17] R. Yogamalar, R. Srinivasan, A. Vinu, K. Ariga, A.C. Bose, Solid State Commun. 149 (2009) 1919.
[18] T. Taniguchi, T. Watanabe, N. Sakamoto, N. Matsushita, Cryst. Growth Des. 8 (2008) 3725.
[19] T. Xia, Q. Li, X. Liu, J. Meng, X. Cao, J. Phys. Chem. B 110 (2006) 2006.
[20] Y. Muraoka, J.C. Grenier, S. Petit, M. Pouchard, Solid State Sci. 1 (1999) 133.
[21] Y. Sun, H. Liu, X. Wang, X. Kong, H. Zhang, Chem. Mater. 18 (2006) 2726.
[22] V.V. Atuchin, T.A. Gavrilova, V.G. Kostrovsky, L.D. Pokrovsky, I.B. Troitskaia, Inorg. Mater. 44 (2008) 622.
[23] S. Jiebing, X. Rui, J. Sol-Gel Sci. Technol. 27 (2003) 315.
[24] L. Jiao, H. Yuan, Y. Si, Y. Wang, M. Zhao, Y. Wang, Mater. Lett. 59 (2005) 3112.
[25] A. Michailovski, F. Krumeich, G.R. Patzke, Chem. Mater. 16 (2004) 1433.
[26] S.R. Dhage, M.S. Hassan, O.B. Yang, Mater. Chem. Phys. 114 (2009) 511.
[27] T. He, J. Yao, J. Photochem. Photobiol. C 4 (2003) 125.
[28] J. Liu, Y. Lu, J. Liu, X. Yang, X. Yu, J. Alloys Compd. 496 (2010) 261.
[29] A. Bouzidi, N. Benramdane, H.T. Derraz, C. Mathieu, B. Khelifa, R. Desfeux, Mater. Sci. Eng. B97 (2003) 5.
[30] V. Nirupama, S. Uthanna, J. Mater. Sci. Mater. Electron. 21 (2010) 45.